





Photon-echo-like phenomenon induced by a phonon

Yongkang Dong ^{1,*}, Chao Pang ^{1,*}, Wuliji Hasi^{1,2}, Liang Chen,³ Xiaoyi Bao ³ and Dengwang Zhou ^{1,2,†}

¹National Key Laboratory of Science and Technology on Tunable Laser, Harbin Institute of Technology, 150001 Harbin, China

²Postdoctoral Research Station for Optical Engineering & Research Center for Space Optical Engineering, Harbin Institute of Technology, Harbin, 150001, China

³Fiber Optics Group, Department of Physics, University of Ottawa, Ottawa, ON K1N 6N5, Canada



(Received 17 April 2022; accepted 9 January 2023; published 6 February 2023)

Photon-phonon interaction is a powerful mechanism for all-optical signal processing, slow (fast) light, microscopy, spectroscopy, microwave photonics, and sensing. Here, we demonstrate a photon-echo-like phenomenon induced by a phonon, whose mechanism is represented by a coherent photon-phonon chain interaction (PPCI) theory referring to the alternating evolution between Stokes scattering and anti-Stokes scattering. An analytical solution, including the impulse response of the coherent PPCI theory, is derived to quantitatively analyze the energy conversion between photon and phonon, showing a damped photoacoustic oscillation. All theoretical analysis, numerical simulation, and experiments confirm that the adjacent order echoes have a phase difference of π , i.e., phase flip, and the echoes generated by using photon and phonon as the initial excitation sources, respectively, are in inverse phase. As a result, the echoes up to the third-order are theoretically analyzed by the proposed coherent PPCI theory and verified by the experiment. This physical mechanism bodes well for a class of photonics applications in telecommunications, optical metrology, and optical computation.

DOI: [10.1103/PhysRevA.107.023504](https://doi.org/10.1103/PhysRevA.107.023504)

I. INTRODUCTION

Photon echo, analogous to spin-echo in magnetic resonance [1], has been studied in the atomic and molecular systems since its first observation [2]. The macroscopic dipole moment created by the first pulse reappears after the second pulse, which reverses the dephasing process and generates a third optical pulse at a delayed time equal to the interval between the first two pulses [3]. It has gained more interest, especially stimulated photon echo, due to its flexibility and applications like optical memory [4–8]. A physical model named transient four-waving mixing theory [9] is used to explain this phenomenon. The first two input pulses engrave a spectral interference in the absorbing medium. The third input pulse sequence interacts with the generated spectral grating, and the sample will radiate a following pulse sequence in time domain.

Photon-phonon interaction especially stimulated Brillouin scattering (SBS) [10], is somewhat related to the generation of the photon-echo-like wave form. In the SBS effect, the interaction between a pump wave (photon) and a Doppler-downshifted Stokes wave excites an acoustic wave (phonon) via electrostriction, which will drive a moving refractive index grating in the material [11,12]. The similar memory behavior of the grating containing the amplitude and phase information of both the two optical waves also promotes its research in optical storage [13–15], slow (fast) light [16–18], pulse compression [19,20], optical signal processing [21–23], sensing [24–26], and microscopy [27–29]. The grating is tunable

[16,30], reconfigurable [31], and refreshable [15] (erasable) [32], resulting in a flexible memory (delay) time. In the case of satisfying the Bragg condition, the acoustic wave can reflect the incident light and generate a retrieval wave form in a frequency-shifting way [13] or polarization separation [22,33] before it is completely relaxed, thus reducing crosstalk. In some special cases [21,22,34], the pump wave form can be well recovered like an echo. However, when the pump and Stokes waves are high in power, corresponding to a strong SBS effect, strong optical spikes emerge behind the injected pump pulse in the time domain, which is induced by residual acoustic wave and dramatically affects its application performance. This process involves the photoacoustic oscillations between the pump wave and the excited acoustic wave, resulting in *photon-echo-like wave forms*, but does not involve the process of dephasing [2].

In this paper, we theoretically analyze and experimentally verify the mechanism of the photon-echo-like phenomenon induced by phonon in optical fiber. In a strong SBS effect where both the pump and Stokes waves are high in power, optical spikes will emerge, stemming from pump photon depletion and phonon depletion. Like stimulated photon echo, the newly generated optical spike can be called zero-order echo. When the SBS effect becomes more vital, first-, second- and higher-order echoes will appear. This kind of echo involves a complex dynamic between the pump photon and the acoustic phonon.

II. COHERENT PHOTON-PHONON CHAIN INTERACTION

The SBS effect is a nonlinear process resulting from the interaction among optical and acoustic waves as the power of the incident light is greater than the stimulated threshold

*These authors contributed equally to this work.

†Corresponding author: dengwangzhou@hit.edu.cn

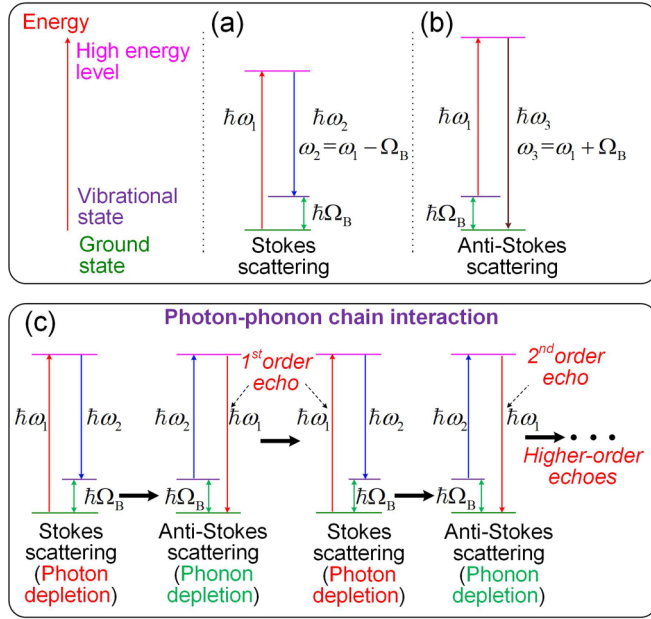


FIG. 1. The energy conservation of stimulated Brillouin scattering. (a) Stokes scattering, (b) anti-Stokes scattering, and (c) coherent PPCI process, in which the Stokes scattering and anti-Stokes scattering occur alternately, generating multiorder echoes.

[35]. From a microscopic point of view, the quantum interpretation of the SBS effect is that the annihilation of an incident photon ($\hbar\omega_1$) produces both a scattered photon ($\hbar\omega_2$) and an excited acoustic phonon ($\hbar\Omega_B$) or the annihilation of an incident photon [$\hbar(\omega_1 - \Omega_B)$] and an existing acoustic phonon ($\hbar\Omega_B$) produce a scattered photon [$\hbar(\omega_1 + \Omega_B)$], which are shown in Figs. 1(a) and 1(b), respectively. Note that the frequency of the scattered photon is lower than that of the incident photon in the former, i.e., *Stokes scattering*, while it is higher than that of the incident photon in the latter, i.e., *anti-Stokes scattering*. Under the strong SBS effect, a more complex interaction occurs. Stokes scattering and anti-Stokes scattering are alternately excited over time, and are called coherent *photon-phonon chain interactions* (PPCIs). As shown in Fig. 1(c), the annihilation of an incident photon ($\hbar\omega_1$) produces both a scattered Stokes photon ($\hbar\omega_2$) and an excited acoustic phonon ($\hbar\Omega_B$) via the Stokes scattering, resulting in a pump photon depletion. Note that the residual incident pump wave can be regarded as a *zero-order echo*. After a complete pump photon depletion, the annihilation of an excited phonon ($\hbar\Omega_B$) and a scattered Stokes photon ($\hbar\omega_2$) will produce an echo photon ($\hbar\omega_1$) (*equivalent pump photon*), i.e., *first-order echo*, via the anti-Stokes scattering, resulting in phonon depletion. After a complete phonon depletion, the annihilation of a *first-echo* photon ($\hbar\omega_1$) will produce both a

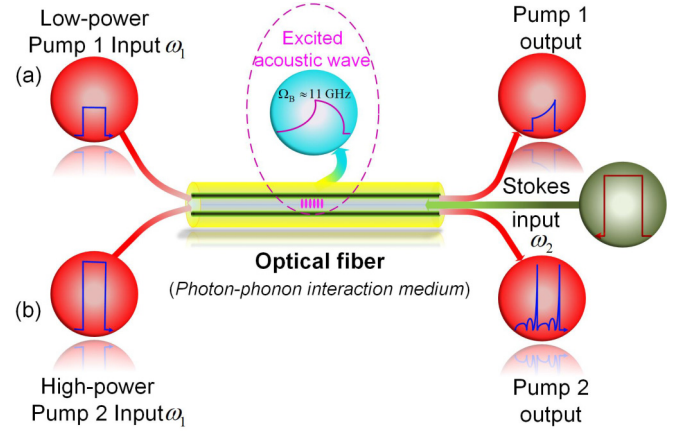


FIG. 2. Demonstration of echoes. (a) Under the weak SBS regime, the output pump pulse shows a decreased amplitude in the time scale. (b) Under a strong SBS regime, the output pump pulse has multiorder echoes.

scattered Stokes photon ($\hbar\omega_2$) and an excited acoustic phonon ($\hbar\Omega_B$), leading to the second pump photon depletion. Furthermore, as the initial pump power increases, *second- and higher-order echoes* will be excited through the alternating chain interaction between the Stokes scattering (pump photon depletion) and the anti-Stokes scattering (phonon depletion), which shows a photoacoustic oscillation.

From a macroscopic point of view, as shown in Fig 2, the coherent PPCI process typically requires a pump wave in the $+z$ direction interacting with a counter-propagated Stokes wave in the $-z$ direction to excite the enhanced acoustic wave. The classical three coupled-wave equations under a slowly-varying amplitude approximation [12,26] can character the proposed coherent PPCI process. For simplicity, the initial and boundary conditions are as follows. The initial pump wave has a square profile $E_1(z, t)|_{z=0} = E_{P0}[u(t) - u(t - w_P)]$, where E_{P0} and w_P are the initial complex field amplitude and width, z is the interaction length, and $u(t)$ is the Heaviside step function. The Stokes wave is a continuous wave. Their powers are at a high level, and the Stokes power P_2 is much larger than the pump peak power P_1 , i.e., $P_1 \ll P_2$. Therefore, it is easy to reach the complete pump photon depletion, and the power fluctuation induced by strong SBS for Stokes wave is negligible, i.e., $E_2(z, t) = E_{S0}$. E_{S0} is the initial complex field amplitude of Stokes wave, and $E_{P0} \ll E_{S0}$. The initial density fluctuation is zero, i.e., $\rho(z, t)|_{t=0} = 0$. Therefore, the simplified coherent PPCI process becomes a linear time-invariant system, and analytic solutions of the evolution of the pump pulse and the acoustic wave in time and space are derived (see Appendix A),

$$\begin{aligned}
 E_1(z, t) &= E_{P0} \left[\delta\left(t - \frac{z}{v_g}\right) + \Gamma u\left(t - \frac{z}{v_g}\right) - \Gamma u\left(t - \frac{z}{v_g} - w_P\right) - \delta\left(t - \frac{z}{v_g} - w_P\right) \right] * [J_0(2\sqrt{Gt})e^{-\Gamma t}] \\
 &= E_{P0} h\left(t - \frac{z}{v_g}\right) + \Gamma E'_1(z, t) * h(t) - E_{P0} h\left(t - \frac{z}{v_g} - w_P\right),
 \end{aligned}
 \tag{1}$$

Term 1
Term 2
Term 3

and

$$\rho(z, t) = ig_1 E_{S0}^* E'_1(z, t) * h(t), \quad (2)$$

where

$$G = g_1 g_2 |E_{S0}|^2 z = \frac{g_1 g_2 P_2 z}{2nc\epsilon_0 A_{\text{eff}}}, \quad (3)$$

$$h(t) = J_0(2\sqrt{Gt})e^{-\Gamma t}, \quad (4)$$

$$E'_1(z, t) = E_{P0} \left[u\left(t - \frac{z}{v_g}\right) - u\left(t - \frac{z}{v_g} - w_p\right) \right]. \quad (5)$$

Here $*$ is the convolution operator, $\delta(t)$ is the Dirac delta function, and $J_0(t)$ is the zero-order Bessel functions of the first kind. $v_g = c/n$ is the group velocity, where c and n are the light velocity in a vacuum and the refractive index, respectively. G is the Brillouin gain factor, as well as the time scale coefficient for the Bessel function $J_0(2\sqrt{Gt})$. Note that $h(t)$ is the *impulse response* and the *intrinsic oscillation profile* of the pump photon and the excited acoustic phonon in the coherent PPCI process. $g_1 = \epsilon_0 \gamma_e (k_1 + k_2)^2 / (2\Omega)$ and $g_2 = \omega_{1,2} \gamma_e / (2nc\rho_0)$ represent the electrostrictive and elasto-optic coupling effects, respectively. ϵ_0 is the vacuum permittivity and $\gamma_e = (n^2 - 1)(n^2 + 2)/3$ is the electrostriction coefficient of optical fiber. k_1 , k_2 and $\vec{q} = \vec{k}_1 + \vec{k}_2$ are the wave number of the pump wave, Stokes wave, and the acoustic wave, respectively, while ω_1 , ω_2 and $\Omega = \omega_1 - \omega_2$ are their angular frequencies. ρ_0 is the mean density of the fiber core. $\Gamma = \Gamma_B/2 - i\Delta\Omega$ is damping acoustic wave coefficient, where Γ_B is the angular Brillouin spectral linewidth whose reciprocal $\tau_p = 1/\Gamma_B$ gives the phonon lifetime (~ 10 ns in standard single-mode fiber), $\Delta\Omega = \Omega - \Omega_B$ is the angular frequency detuning, and Ω_B is the angular Brillouin frequency shift. The relation between optical power and optical field is $P_{1,2} = 2nc\epsilon_0 A_{\text{eff}} |E_{1,2}|^2$, where A_{eff} is the effective area of the optical field. Then, $H(z, s)$ is the transfer function of the coherent PPCI process, and s is the complex frequency variable. $E'_1(z, t)$ represents the evolution of pump pulse along the fiber without the SBS effect. Equation (1) shows that the evolution of the pump pulse along the fiber is a convolution of the pump pulse profile $E_1(z, t)|_{t=0^+}$ at the time $t = 0^+$ with the impulse response $h(t)$. Two unit impulse functions (Dirac delta functions) $\delta(t - z/v_g)$ and $-\delta(t - z/v_g - w_p)$ are induced by the rising edge and the falling edge of the pump pulse. Consequently, the evolution profile of the pump pulse is made up of three terms.

The evolution of a 30-ns pump pulse along a 10-m standard single-mode fiber interacting with a continuous Stokes wave via the SBS effect is numerically simulated based on Eq. (1), which is demonstrated in Fig. 3(a). As the interaction distance increases, the middle segment of the pump pulse is quickly absorbed. At the same time, two high-power spikes with attenuated oscillations appear at both the front and the end of the pump pulse emerge. The corresponding acoustic wave is demonstrated in Fig. 3(b). The amplitude of the acoustic wave in Eq. (2) is proportional to the term 2 of the right-hand side in Eq. (1); hereafter, we focus only on the evolution of the pump pulse.

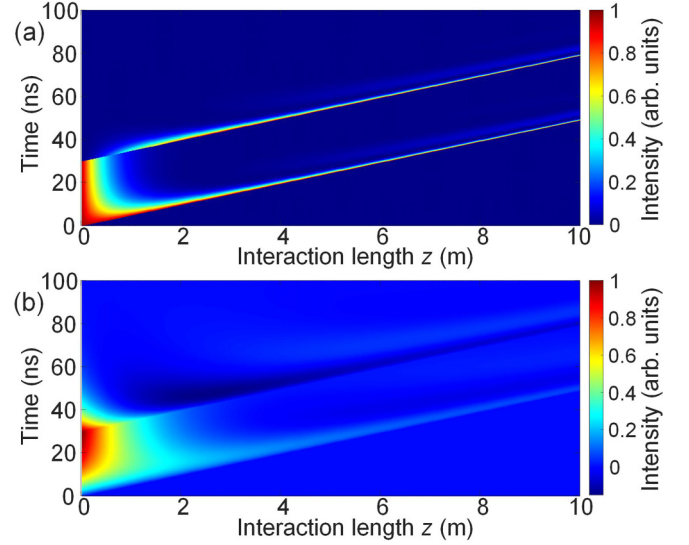


FIG. 3. Analytical solutions' spatial and temporal evolution along a 10-m standard single-mode fiber for (a) the pump pulse and (b) the acoustic wave.

Then, the wave forms of the terms of the right-hand side in Eq. (4) and Eq. (1) with the interaction length ranging from 0.56 m to 10 m are illustrated in Figs. 4(a), 4(c), 4(e), and 4(g) and 4(b), 4(d), 4(f), 4(h), respectively. At an interaction length $z = 0.56$ m with the Brillouin gain factor $G = 6.13 \times 10^7$ Ns/kg, the main peak and the first trough of the Bessel function $J_0(2\sqrt{Gt})$ (red short-dashed line) appear within 120 ns, whose wave form is confined by an exponential decay $\exp(-\Gamma t)$ (black dashed-dotted line), as shown in Fig. 4(a). Therefore, the impulse response $h(t)$ (blue line) decreases to zero line (green dashed line), offering a complete pump photon depletion. The main peak of $h(t)$ can be regarded as the intrinsic zero-order echo. Then, the output wave form without PPCI (black dashed line) is a standard 30-ns square pulse, while the output wave form with PPCI (blue line) gradually decays with a tail behind the rear pulse, which are shown in Fig. 4(b). The residual front edge and the regenerated tail can be regarded as compound zero-order echoes because they are the sum of three terms: $E_{P0}h(t - z/v_g)$ (red dotted line), $\Gamma E'_1(z, t) * h(t)$ (magenta short-dashed line), and $-E_{P0}h(t - z/v_g - w_p)$ (orange dashed-dotted line). Note that the first and third terms have the same profile but a phase difference π while the second term gradually increases to saturation within a pump pulse width of 30 ns, and then quickly decreases due to the finite phonon lifetime. When the interaction length z is increased to 2.40 m, corresponding to a Brillouin gain factor $G = 2.63 \times 10^8$ Ns/kg, the first peak and the second trough of the Bessel function $J_0(2\sqrt{Gt})$ appears, as shown in Fig. 4(c), so that the first trough, i.e., the intrinsic first order echo of $h(t)$ is excited due to the phonon depletion. The negative value indicates an inverse phase $1 \cdot \pi$ compared to the intrinsic zero-order echo, showing the first phase flip. The zero and pole points of $h(t)$ correspond to the complete photon depletion and the complete phonon depletion, respectively. Subsequently, the intrinsic first-order echo will experience photon depletion until its amplitude returns to zero. As shown

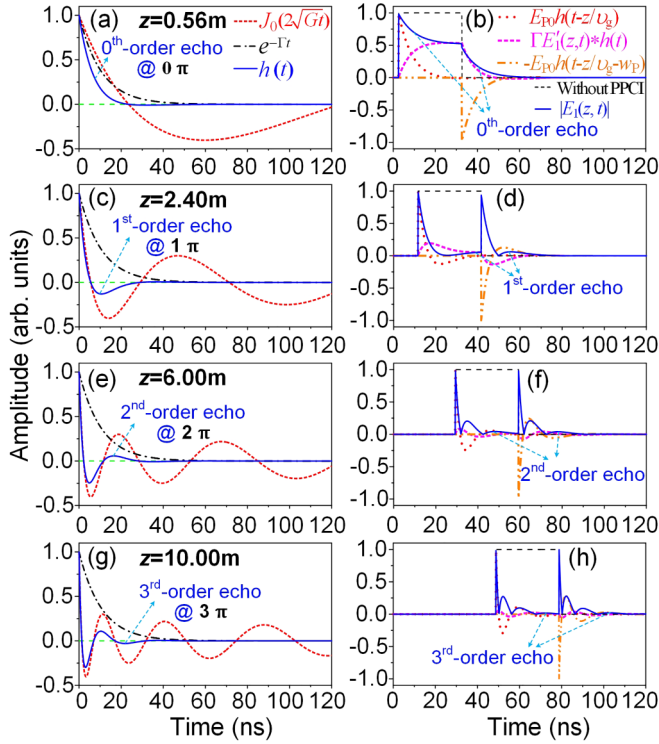


FIG. 4. Demonstration of echoes. The Bessel function $J_0(2\sqrt{Gt})$ (red short-dashed line), $\exp(-\Gamma t)$ (black dashed-dotted line), and their product $h(t)$ (blue line) of Eq. (4) are plotted at (a) $z = 0.56$ m, (c) $z = 2.40$ m, (e) $z = 6.00$ m and (g) $z = 10.00$ m, respectively. Three terms and the output pump pulse without/with PPCL of Eq. (1) are plotted at (b) $z = 0.56$ m, (d) $z = 2.40$ m, (f) $z = 6.00$ m, and (h) $z = 10.00$ m, respectively.

in Fig. 4(d), the corresponding amplitudes of the three terms in Eq. (1) decrease quickly, resulting in two optical spikes, i.e., the compound zero-order echoes, and two flatter peaks, i.e., compound first-order echoes. If z increases to 6.00 m corresponding to $G = 6.57 \times 10^8$ Ns/kg, both the intrinsic and the compound second-order echoes emerge due to the phonon depletion shown in Figs. 4(e) and 4(f), respectively. The phase of the intrinsic second-order echo is 2π , i.e., the second phase flip. After a complete phonon depletion, the second-order echoes will experience the photon depletion until their amplitude returns to zero. Finally, the intrinsic and the compound echoes of up to third-order with a phase of 3π , i.e., third phase flip, are apparent at $z = 10.00$ m and $G = 1.10 \times 10^9$ Ns/kg, shown in Figs. 4(g) and 4(h), respectively. Since the first term and the third term in Eq. (1) are in the inverse phase, the excitation source of the first term can be regarded as the incident pump photon, while that of the third term is the excited phonon.

III. EXPERIMENT DESCRIPTION AND RESULTS

An experiment is performed in Fig. 5. The light output from a narrow linewidth laser at 1550 nm and 20 mW is split into three branches. The upper blue branch is used for generating the pump pulse. The light carrier is first frequency-shifted using an electro-optic modulator (EOM1) with an RF

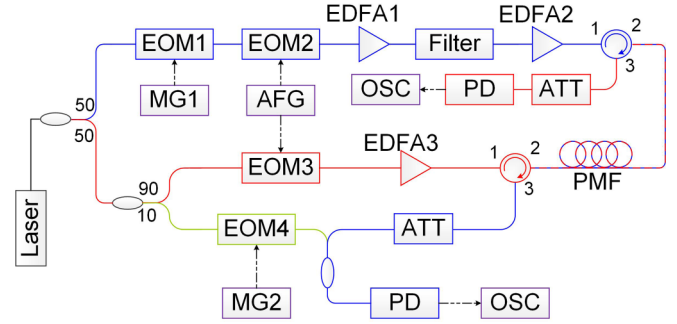


FIG. 5. Apparatus for measurement of echoes induced by phonon in optical fiber. EOM, electro-optic modulator; EDFA, erbium-doped fiber amplifier; MG, microwave generator; AFG, arbitrary function generator; ATT, attenuator; PD, photodetector; OSC, oscilloscope; PMF, polarization-maintaining fiber.

frequency of 10.845 GHz, exactly the Brillouin frequency shift of the used polarization-maintaining fiber (PMF), and then amplitude-modulated into an optical square pulse using EOM2. The upper-frequency sideband is selected by an optical filter. As a result, the frequency of the pump pulse is 10.845-GHz higher than that of the optical carrier. The optical pump pulse is amplified by two erbium-doped fiber amplifiers (EDFAs) to several watts. It then is launched into a 15-m PMF fiber, i.e., photon-phonon medium, from one end. Since amplifying the continuous wave to several watts with the EDFA in our laboratory is challenging, the light in the middle red branch is modulated by EOM3 to another square pulse and amplified by EDFA3 to a peak power of several Watts. It is injected into the PMF from the other end as the Stokes wave. The lower green branch, modulated by EDFA4 with a 12.145-GHz RF signal, acts as the reference wave in heterodyne detection. A 1.3-GHz heterodyne signal between the output pump wave and the reference wave is converted to an electric signal by a 1.6-GHz photodetector (PD) and acquired by a 10-GSa/s oscilloscope. Finally, the acquired heterodyne signal is processed by in-phase and quadrature (I/Q) demodulation algorithm [36] to obtain both the amplitude and the phase of the output pump pulse. The polarization state of the two optical pulses is adjusted to the slow axis of the PMF fiber to avoid polarization fading.

The evolution of the pump pulse (30 ns @ 11.5 W) is demonstrated in Fig. 6(a), with the peak power of a 30-ns Stokes pulse ranging from 0 W to 11.3 W. The main body of the pump pulse is gradually absorbed. A residual optical spike remains at the front. In contrast, a new optical spike emerges behind the falling edge of the pump pulse, which corresponds to the compound zero-order echoes as described in Sec. II. As the Stokes pulse power further increases beyond 2 W, the compound first-order echo is slightly excited. For a relatively weak SBS effect, the input pump pulse (30 ns @ 6.2 W) and Stokes pulse (30 ns @ 3.7 W) are shown by red dashed lines in Fig. 6(b) and 6(d), respectively. In this scenario, two zero-order echoes are observed at the front end and behind the back end of the output pump pulse (blue line). The numerical simulation (black dashed-dotted line) [37,38] is in good agreement with the experimental result, while the analytic solution (magenta dotted line) based on Eq. (1) also

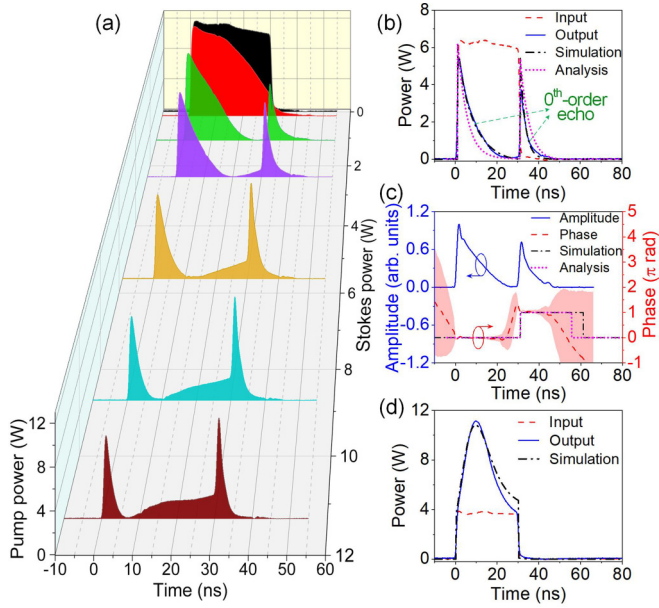


FIG. 6. Observation of echoes under a weak SBS effect. (a) The evolution of the output pump pulse as the Stokes pulse power ranges from 0 W to 11.3 W. (b) The input pump pulse (red dashed line), the output pump pulse (blue line), the simulation result (black dashed-dotted line), and the analytic solution (magenta dotted line). (c) The heterodyne detection and the IQ demodulation algorithm obtain the amplitude (blue line) and the phase (red dashed line) of the output pump pulse. The red band errors are the standard deviation of repeat measurements. Black dashed-dotted line and magenta dot line are the phase distributions of the numerical simulation and the analytic solution, respectively. (d) The input Stokes pulse (red dash line), the output Stokes pulse (blue line), and the numerical simulation result (black dashed-dotted line).

shows two optical spikes. The discrepancy may originate from the simplicity of our theoretical model, which neglects the fluctuations of the Stokes wave. As shown in Fig. 6(c), the amplitude (blue line) and phase (red dashed line) of the output pump pulse are calculated by the IQ demodulation. It can be seen that a π -phase shift is demonstrated between the front zero-order echo and the back zero-order echo, which is consistent with the numerical simulation (black dashed-dotted line) and the analytic solution (magenta dotted line). The standard deviation (red band) is computed, showing more uncertainty when the amplitude approaches zero. As shown in Fig. 6(d), the Stokes pulse is amplified by the pump pulse via Brillouin amplification, resulting in a higher peak for both the experimental result (blue line) and the numerical simulation (black dashed-dotted line). The newly generated high-power peak contributes to the difference between the experimental result and the analytic solution for the pump pulse.

Next, the pump pulse (30 ns @ 13.1 W) and the Stokes pulse (70 ns @ 6.7 W) are used to excite a higher-order echo for a strong SBS effect. As shown in Fig. 7(a), both the zero- and first-order echoes are excited in the output pump pulse, as well as the numerical simulation and the analytic solution. As shown in Fig. 7(b), the first-order echo has a π -phase shift compared to the zero-order echo, i.e., the first phase flip. Both zero- and first-order echoes within the pump pulse have a

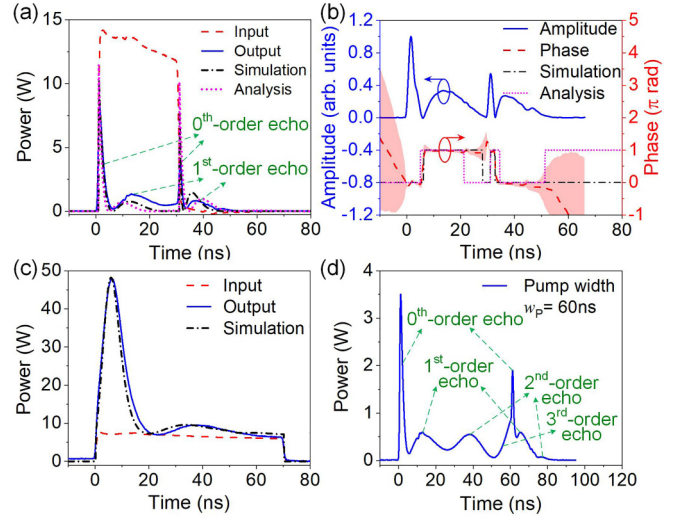


FIG. 7. Observation of multiorder echoes under a strong SBS effect. (a), (c) The input and output shapes of the pump and Stokes waves. The red dashed lines are the input pulses. The blue lines are the output wave forms. The black dashed-dotted lines are calculated by numerical simulation. The magenta dotted line is the analytic solution. (b) The output pump pulse's amplitude (blue line) and phase (red dashed line). The red band is the standard deviation of repeat measurements. Black dashed-dotted line and magenta dotted line are the phase distributions of the numerical simulation and the analytic solution, respectively. (d) second- and third-order echoes are excited by using 60-ns pulses.

π -phase shift compared to those behind the falling edge of the pump pulse, i.e., the inverse phase relation. In addition, the power fluctuation of the output Stokes pulse in Fig. 7(c) is induced by energy transfer in alternating the pump photon depletion and the phonon depletion because the excited phonon and the Stokes photon are produced and annihilated in pairs. Using a pulse width of 60 ns for both pump pulse and Stokes pulse to increase the interaction length, second-order and even third-order echoes are also excited, as illustrated in Fig. 7(d). More details are discussed in Appendixes B and C.

IV. DISCUSSION

Although the phenomenon of zero-order echo has been mentioned in previous research [34], they give an incomplete hypothesis: these two optical spikes of the output pump pulse are the residual of the pump pulse because both fast rising and falling edges (containing abundant high-frequency components) of the pump pulse cannot be fully absorbed due to the insufficient SBS bandwidth. However, it should be pointed out that the falling edge can be fully eliminated, and the second optical spike is behind (not within) the falling edge of the pump pulse, which their hypothesis cannot explain. In our opinion, the front zero-order echo is the residual component of the rising edge of the pump pulse since it takes several nanoseconds to establish a strong acoustic wave, while the excited photons induce the other echoes through anti-Stokes scattering. The initial excitation source of the echoes within the pump pulse is the pump photon, while the echoes behind

the falling edge of the pump pulse are the excited phonon. Therefore, they have the inverse phase (see Appendix C).

In addition, the combination of the PMF fiber and the Stokes wave is equivalent to an optical high-pass filter. The high-frequency component of the pump pulse within the bandwidth of the high-pass filter can be passed through this filter, and the oscillation of output echoes is similar to the *Gibbs-Wilbraham phenomenon* [39] in electrical filters.

With a higher power Stokes wave or a longer interaction length, an equivalent strong SBS interaction can generate higher-order echoes. For a variety of modulated pump-Stokes wave forms, a more general formula of Eq. (4) is derived as follows:

$$h_g(t) = J_0[2\sqrt{G(z, t)t}]e^{-\Gamma t} \cdot E_2(z, t), \quad (6)$$

where $G(z, t)$ is determined by the powers and the duration (interaction length) of the pump and Stokes waves. In addition, the peak power of the back zero-order echo is sometimes higher than the former due to the accumulation of the phonon, which may provide a new ideal for the generation or amplification of the high-power optical pulse.

V. CONCLUSIONS

We have theoretically analyzed and experimentally verified the physical mechanism of the photon-echo-like phenomenon induced by phonon. A coherent PPCI theory is proposed to describe the mechanism, which involves the alternating evolution of the Stokes scattering and the anti-Stokes scattering over time. With a simplified mathematical model of the coherent PPCI theory, an analytical solution is derived to demonstrate echoes and to quantitatively analyze the energy conversion between the pump photon and the excited phonon. Based on the theoretical analysis, the numerical simulation, and the experiment, we summarize the following inferences: the adjacent order echoes have a phase difference of π , i.e., phase flip; The echoes emitted using the incident pump photon and the excited phonon as the initial excitation sources, respectively, are the inverted phase. We believe that the photon-echo-like phenomenon induced by phonon offers an approach to exploring the fundamental dynamics in a strong photon-phonon interaction system.

ACKNOWLEDGMENTS

This work is supported by the National Natural Science Foundation of China (No. 62005067), China National Postdoctoral Program for Innovative Talents (No. BX20200104), China Postdoctoral Science Foundation (No. 2020M681088), and the Heilongjiang Postdoctoral Fund to pursue scientific research in Heilongjiang Province (No. LBH-Z20067). It is also supported by the Scientific Research Foundation for Postdoctoral Teacher of Harbin Institute of Technology (No. AUGA5630100120).

Y.D. supervised the project. Y.D., C.P., and D.Z., initiated and conceived the research. D.Z. developed the theoretical analysis and mathematical model. C.P. performed experiments and a partial phenomenon explanation. C.P., and D.Z. performed numerical simulation. C.P., D.Z., and Y.D. drafted and

revised the manuscript. All authors participated in discussions during the drafting of the manuscript.

APPENDIX A: ANALYTIC SOLUTION OF COHERENT PPCI THEORY

The coherent PPCI theory involves the process of three-wave coupling, i.e., two optical waves that can be described by Maxwell's set of equations and acoustic waves described by the material equations. Since the laser wavelength used in this experiment is $\lambda = 1550$ nm, The space and time scales of the complex amplitude E_1 , E_2 , and ρ varies are generally much longer than the wavelength and the period of the carrier wave, respectively. The rising and falling edges of the pulses in the experiment are on the order of nanoseconds, much larger than the period of the carrier wave. The time step and space step of the numerical simulation and the analytical solution is much longer than the carrier wave's wavelength and period. Therefore, a slowly-varying amplitude approximation [12,40] is satisfied, and the second-order derivative terms of the optical and acoustic waves can be neglected, i.e., $|\partial^2 E_{1,2}/\partial t^2| \ll |\omega_{1,2}\partial E_{1,2}/\partial t|$, $|\partial^2 E_{1,2}/\partial z^2| \ll |k_{1,2}\partial E_{1,2}/\partial z|$, and $|\partial^2 \rho/\partial t^2| \ll |\Omega\partial \rho/\partial t|$. In addition, the propagation distance of the acoustic phonon is on the order of microns before being absorbed so that the term $|\partial \rho/\partial z|$ is negligible. As a result, the mathematical model of the coherent PPCI theory is given by Refs. [12,26],

$$\frac{\partial E_1(z, t)}{\partial z} + \frac{1}{v_g} \frac{\partial E_1(z, t)}{\partial t} = ig_2 E_2(z, t) \rho(z, t), \quad (A1)$$

$$-\frac{\partial E_2(z, t)}{\partial z} + \frac{1}{v_g} \frac{\partial E_2(z, t)}{\partial t} = ig_2 E_1(z, t) \rho^*(z, t), \quad (A2)$$

$$\frac{\partial \rho(z, t)}{\partial t} + \Gamma \rho(z, t) = ig_1 E_1(z, t) E_2^*(z, t). \quad (A3)$$

For simplicity, the initial and boundary conditions are as follows:

$$E_1(z, t)|_{z=0} = E_{P0}[u(t) - u(t - w_P)], \quad (A4)$$

$$E_1(z, t)|_{t=0^-} = 0, \quad (A5)$$

$$E_2(z, t) = E_{S0}, \quad (A6)$$

$$\rho(z, t)|_{t=0^-} = 0. \quad (A7)$$

After these assumptions, the coherent PPCI process becomes a linear time-invariant system. Then, the Laplace transforms of Eqs. (A1) and (A3) are expressed as

$$\frac{\partial \tilde{E}_1(z, s)}{\partial z} + \frac{1}{v_g} [s\tilde{E}_1(z, s) - E_1(z, t)|_{t=0^-}] = ig_2 E_{S0} \tilde{\rho}(z, s), \quad (A8)$$

$$s\tilde{\rho}(z, s) - \rho(z, t)|_{t=0^-} + \Gamma \tilde{\rho}(z, s) = ig_1 \tilde{E}_1(z, s) E_{S0}^*. \quad (A9)$$

Substituting Eq. (A7) into Eq. (A9), we will obtain the formula,

$$\tilde{\rho}(z, s) = \frac{ig_1}{s + \Gamma} \tilde{E}_1(z, s) E_{S0}^*. \quad (A10)$$

Substituting Eq. (A5) and Eq. (A10) into Eq. (A8), we will obtain the formula,

$$\frac{\partial \tilde{E}_1(z, s)}{\partial z} = \left[-\frac{g_1 g_2}{s + \Gamma} |E_{S0}|^2 - \frac{1}{v_g} s \right] \tilde{E}_1(z, s). \quad (A11)$$

Equation (A11) is a homogeneous differential equation of the first order, and its general solution is given by

$$\begin{aligned} \tilde{E}_1(z, s) &= C \times \exp \left[-\int \left(\frac{g_1 g_2}{s + \Gamma} |E_{S0}|^2 + \frac{1}{v_g} s \right) dz \right] \\ &= C \times \exp \left[-\left(\frac{g_1 g_2}{s + \Gamma} |E_{S0}|^2 + \frac{1}{v_g} s \right) z \right], \end{aligned} \quad (A12)$$

where \times is the multiplication operator. From Eq. (A12), we can find the formula $\tilde{E}_1(z, s)|_{z=0^-} = C$ when the interaction distance is $z = 0$. Considering the boundary condition of Eq. (A4), its Laplace transform is expressed as

$$\begin{aligned} \tilde{E}_1(z, s)|_{z=0^-} &= E_{P0} \times \mathcal{L}\{u(t) - u(t - w_p)\} \\ &= E_{P0} \times \left[\frac{1}{s} - \frac{\exp(-w_p s)}{s} \right], \end{aligned} \quad (A13)$$

where $\mathcal{L}\{\cdot\}$ is the operator of the Laplace transform. Then,

$$C = E_{P0} \times \left[\frac{1}{s} - \frac{\exp(-w_p s)}{s} \right]. \quad (A14)$$

Substituting Eq. (A14) into Eq. (A12), the Laplace transform of the evolution of the pump pulse is obtained as

$$\begin{aligned} \tilde{E}_1(z, s) &= E_{P0} \left[\frac{1}{s} - \frac{\exp(-w_p s)}{s} \right] \times \exp \left(-\frac{g_1 g_2 |E_{S0}|^2 z}{s + \Gamma} \right) \times \exp \left(-\frac{z}{v_g} s \right) \\ &= E_{P0} \left[\exp \left(-\frac{z}{v_g} s \right) - \exp \left(-\frac{z}{v_g} s - w_p s \right) \right] \left(1 + \frac{\Gamma}{s} \right) \times \frac{1}{s + \Gamma} \exp \left(-\frac{G}{s + \Gamma} \right) \\ &= E_{P0} \times \mathcal{L} \left\{ \delta \left(t - \frac{z}{v_g} \right) - \delta \left(t - \frac{z}{v_g} - w_p \right) + \Gamma u \left(t - \frac{z}{v_g} \right) - \Gamma u \left(t - \frac{z}{v_g} - w_p \right) \right\} \times \mathcal{L}\{\exp(-\Gamma t) J_0(2\sqrt{Gt})\}, \end{aligned} \quad (A15)$$

where

$$G = g_1 g_2 |E_{S0}|^2 z = g_1 g_2 \frac{P_2}{2nc\epsilon_0 A_{\text{eff}}} z. \quad (A16)$$

Substituting Eq. (A15) into Eq. (A10), the Laplace transform of the evolution of the acoustic wave is given by

$$\begin{aligned} \tilde{\rho}(z, s) &= \frac{ig_1}{s + \Gamma} E_{P0} \times \left[\frac{1}{s} - \frac{\exp(-w_p s)}{s} \right] \times \exp \left(-\frac{g_1 g_2}{s + \Gamma} |E_{S0}|^2 z \right) \times \exp \left(-\frac{z}{v_g} s \right) \\ &= ig_1 E_{P0} E_{S0}^* \times \left[\exp \left(-\frac{z}{v_g} s \right) - \exp \left(-\frac{z}{v_g} s - w_p s \right) \right] \frac{1}{s} \times \frac{1}{s + \Gamma} \exp \left(-\frac{G}{s + \Gamma} \right) \\ &= ig_1 E_{P0} E_{S0}^* \times \mathcal{L} \left\{ u \left(t - \frac{z}{v_g} \right) - u \left(t - \frac{z}{v_g} - w_p \right) \right\} \times \mathcal{L}\{\exp(-\Gamma t) J_0(2\sqrt{Gt})\}. \end{aligned} \quad (A17)$$

Then, the most critical step of the solving process is based on the following Laplace transform identity:

$$\mathcal{L}\{J_0(2\sqrt{at})\} = \frac{1}{s} e^{-\frac{a}{s}}, \quad (A18)$$

where $J_0(t)$ is the zero-order Bessel functions of the first kind and a is the time scale coefficient. Consequently, Eq. (A15) and Eq. (A17) can be solved as

$$\begin{aligned} E_1(z, t) &= E_{P0} \left[\delta \left(t - \frac{z}{v_g} \right) + \Gamma u \left(t - \frac{z}{v_g} \right) - \Gamma u \left(t - \frac{z}{v_g} - w_p \right) - \delta \left(t - \frac{z}{v_g} - w_p \right) \right] * J_0(2\sqrt{Gt}) e^{-\Gamma t} \\ &= E_{P0} h \left(t - \frac{z}{v_g} \right) + \Gamma E'_1(z, t) * h(t) - E_{P0} h \left(t - \frac{z}{v_g} - w_p \right), \end{aligned} \quad (A19)$$

Term 1 Term 2 Term 3

and

$$\rho(z, t) = ig_1 E_{P0} E_{S0}^* \left[u \left(t - \frac{z}{v_g} \right) - u \left(t - \frac{z}{v_g} - w_p \right) \right] * [J_0(2\sqrt{Gt}) e^{-\Gamma t}] = ig_1 E_{S0}^* E'_1(z, t) * h(t), \quad (A20)$$

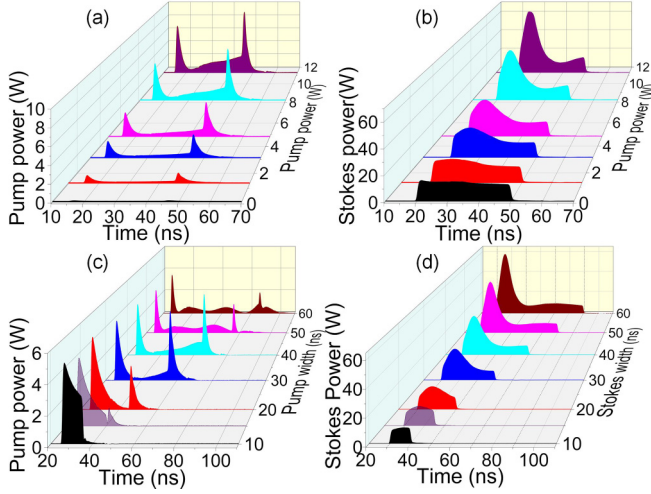


FIG. 8. Experimental results of the output pump pulse and the output Stokes pulse for different power and width. (a), (b) Pump power is increased from 0 W to 11.3 W. (c), (d) The width of both pump pulse and Stokes pulse is tuned from 10 ns to 60 ns.

where

$$h(t) = J_0(2\sqrt{Gt})e^{-\Gamma t}, \quad (\text{A21})$$

$$H(z, s) = \frac{1}{s + \Gamma} \exp\left(-\frac{G}{s + \Gamma}\right), \quad (\text{A22})$$

$$E'_1(z, t) = E_{P0} \left[u\left(t - \frac{z}{v_g}\right) - u\left(t - \frac{z}{v_g} - w_p\right) \right]. \quad (\text{A23})$$

The symbol $*$ is the convolution operator, $\delta(t)$ is the Dirac delta function, and G is the *Brillouin gain factor* or the time scale coefficient of the $J_0(2\sqrt{Gt})$. $h(t)$ and $H(z, s)$ are the *impulse response* and the transfer function of the coherent PPCI process, respectively, and s is the complex frequency variable. $E'_1(z, t)$ represents the evolution of the pump pulse along with the fiber without the SBS effect.

APPENDIX B: EXTENDED EXPERIMENT OF PHOTON-ECHO-LIKE PHENOMENON

The influence of the power and width of the pump pulse and Stokes pulse is investigated in Fig. 8. With the pump power ranging from 0 W to 11.3 W, the evolutions of the output pump pulse and the output Stokes pulse are shown in Figs. 8(a) and 8(b), respectively. The zero-order echo is gradually enhanced, and the first-order echo is excited for the pump pulse while the Stokes pulse is amplified, resulting in a high-power peak due to Brillouin amplification. Then, the widths of the pump pulse and the Stokes pulse are synchronously tuned from 10 ns to 60 ns, as shown in Fig. 8(c) and 8(d), zero-, first-, second- and even third-order echoes for the output pump pulse can also be excited while the output Stokes pulse is amplified via Brillouin amplification resulting in a high power spike and a flatter peak. It can be concluded that the Brillouin gain factor $G(z, t)$ is improved by increasing the power and the width (corresponding to the interaction length) of both the pump and Stokes wave forms, thus obtaining higher-order echoes, which is consistent with the Eq. (6).

APPENDIX C: PHASE INFORMATION OF WAVES

The initial phases of pump and Stokes waves are set as φ_1 and φ_2 , respectively, so that the phase of the excited acoustic wave can be calculated to be $\varphi_1 - \varphi_2 + \pi/2$ based on the right term $ig_1E_1(z, t)E_2^*(z, t)$ of the Eq. (A3). Note that the excited acoustic will interact with the existing pump wave and the Stokes wave, resulting in the regenerated Stokes wave and pump wave, and their phases can be calculated to be φ_2 and $\varphi_1 - \pi$ (right part of the arrow in Table I) based on the right term $ig_2E_1(z, t)\rho^*(z, t)$ of the Eq. (A2) and the right term $ig_2E_2(z, t)\rho(z, t)$ of the Eq. (A1), respectively. The phase relation shows that the pump wave will be quickly absorbed, and the Stokes wave is amplified. Then, the phase relationship between the optical and acoustic waves is calculated for the coherent PPCI. Tables I and II correspond to the initial excitation sources as the input pump photon and the excited phonon, respectively.

TABLE I. Phase information of optical and acoustic waves when the initial excitation source is the incident pump photon.

Waves	Zero-order echo			First-order echo			Second-order echo				
	Initial	Photon depletion	Complete photon depletion	Phonon depletion	Complete phonon depletion	Photon depletion	Complete photon depletion	Phonon depletion	Complete phonon depletion	Photon depletion	Complete photon depletion
Pump	φ_1	$\varphi_1 \leftarrow \varphi_1 + \pi$	—	$\varphi_1 + \pi$	$\varphi_1 + \pi$	$\varphi_1 + \pi \leftarrow \varphi_1$	—	φ_1	φ_1	$\varphi_1 \leftarrow \varphi_1 + \pi$	—
Stokes	φ_2	$\varphi_2 \leftarrow \varphi_2$	φ_2	$\varphi_2 \leftarrow \varphi_2 + \pi$	φ_2	$\varphi_2 \leftarrow \varphi_2$	φ_2	$\varphi_2 \leftarrow \varphi_2 + \pi$	φ_2	$\varphi_2 \leftarrow \varphi_2$	φ_2
Acoustic	—	$\varphi_1 - \varphi_2 + \frac{\pi}{2}$	$\varphi_1 - \varphi_2 + \frac{\pi}{2}$	$\varphi_1 - \varphi_2 + \frac{\pi}{2}$ $\leftarrow \varphi_1 - \varphi_2 - \frac{\pi}{2}$	—	$\varphi_1 - \varphi_2 - \frac{\pi}{2}$	$\varphi_1 - \varphi_2 - \frac{\pi}{2}$	$\varphi_1 - \varphi_2 - \frac{\pi}{2}$ $\leftarrow \varphi_1 - \varphi_2 + \frac{\pi}{2}$	—	$\varphi_1 - \varphi_2 + \frac{\pi}{2}$	$\varphi_1 - \varphi_2 + \frac{\pi}{2}$

TABLE II. Phase information of optical and acoustic waves when the initial excitation source is the excited phonon.

Waves	Zero-order echo				First-order echo				
	Initial phase	Phonon depletion	Complete phonon depletion	Photon depletion	Complete photon depletion	Phonon depletion	Complete phonon depletion	Photon depletion	Complete photon depletion
Pump	—	$\varphi_1 + \pi$	$\varphi_1 + \pi$	$\varphi_1 + \pi \leftarrow \varphi_1$	—	φ_1	φ_1	$\varphi_1 \leftarrow \varphi_1 + \pi$	—
Stokes	φ_2	$\varphi_2 \leftarrow \varphi_2 + \pi$	φ_2	$\varphi_2 \leftarrow \varphi_2$	φ_2	$\varphi_2 \leftarrow \varphi_2 + \pi$	φ_2	$\varphi_2 \leftarrow \varphi_2$	φ_2
Acoustic	$\varphi_1 - \varphi_2 + \frac{\pi}{2}$	$\varphi_1 - \varphi_2 + \frac{\pi}{2}$ $\leftarrow \varphi_1 - \varphi_2 - \frac{\pi}{2}$	—	$\varphi_1 - \varphi_2 - \frac{\pi}{2}$	$\varphi_1 - \varphi_2 - \frac{\pi}{2}$	$\varphi_1 - \varphi_2 - \frac{\pi}{2}$ $\leftarrow \varphi_1 - \varphi_2 + \frac{\pi}{2}$	—	$\varphi_1 - \varphi_2 + \frac{\pi}{2}$	$\varphi_1 - \varphi_2 + \frac{\pi}{2}$

- [1] E. L. Hahn, *Phys. Rev.* **80**, 580 (1950).
- [2] N. A. Kurnit, I. D. Abella, and S. R. Hartmann, *Phys. Rev. Lett.* **13**, 567 (1964).
- [3] I. D. Abella, N. A. Kurnit, and S. R. Hartmann, *Phys. Rev.* **141**, 391 (1966).
- [4] M. Mitsunaga, *Opt. Quant. Electron.* **24**, 1137 (1992).
- [5] X. A. Shen, A.-D. Nguyen, J. W. Perry, D. L. Huestis, and R. Kachru, *Science* **278**, 96 (1997).
- [6] S. A. Moiseev and B. S. Ham, *Phys. Rev. A* **70**, 063809 (2004).
- [7] W. Tittel, M. Afzelius, T. Chanelière, R. L. Cone, S. Kröll, S. A. Moiseev, and M. Sellars, *Laser Photonics Rev.* **4**, 244 (2010).
- [8] D. L. McAuslan, P. M. Ledingham, W. R. Naylor, S. E. Beavan, M. P. Hedges, M. J. Sellars, and J. J. Longdell, *Phys. Rev. A* **84**, 022309 (2011).
- [9] P. Ye and Y. R. Shen, *Phys. Rev. A* **25**, 2183 (1982).
- [10] L. Brillouin, *Ann. Phys. (Paris)* **9**, 88 (1922).
- [11] G. P. Agrawal, *Nonlinear Fiber Optics* (Elsevier Academic Press, Amsterdam, 2007), 4th ed.
- [12] R. W. Boyd, in *Nonlinear Optics* (Academic Press, Burlington, Canada, 2008), p. 429.
- [13] V. P. Kalosha, W. Li, F. Wang, L. Chen, and X. Bao, *Opt. Lett.* **33**, 2848 (2008).
- [14] C.-H. Dong, Z. Shen, C.-L. Zou, Y.-L. Zhang, W. Fu, and G.-C. Guo, *Nat. Commun.* **6**, 6193 (2015).
- [15] B. Stiller, M. Merklein, C. Wolff, K. Vu, P. Ma, S. J. Madden, and B. J. Eggleton, *Optica* **7**, 492 (2020).
- [16] Y. Okawachi, M. S. Bigelow, J. E. Sharping, Z. Zhu, A. Schweinsberg, D. J. Gauthier, R. W. Boyd, and A. L. Gaeta, *Phys. Rev. Lett.* **94**, 153902 (2005).
- [17] M. González-Herráez, K.-Y. Song, and L. Thévenaz, *Appl. Phys. Lett.* **87**, 081113 (2005).
- [18] L. Thevenaz, *Nat. Photonics* **2**, 474 (2008).
- [19] D. T. Hon, *Opt. Lett.* **5**, 516 (1980).
- [20] X. Long, W. Zou, and J. Chen, *Opt. Express* **24**, 5162 (2016).
- [21] S. Chin and L. Thévenaz, *Laser Photonics Rev.* **6**, 724 (2012).
- [22] M. Santagiustina, S. Chin, N. Primerov, L. Ursini, and L. Thévenaz, *Sci. Rep.* **3**, 1594 (2013).
- [23] M. A. Soto, A. Denisov, X. Angulo-Vinuesa, S. Martin-Lopez, L. Thévenaz, and M. Gonzalez-Herraez, *Opt. Lett.* **42**, 2539 (2017).
- [24] A. Denisov, M. A. Soto, and L. Thevenaz, *Light: Sci. Appl.* **5**, e16074 (2016).
- [25] Y. Mizuno, N. Hayashi, H. Fukuda, K. Y. Song, and K. Nakamura, *Light: Sci. Appl.* **5**, e16184 (2016).
- [26] D. Zhou, Y. Dong, B. Wang, C. Pang, D. Ba, H. Zhang, Z. Lu, H. Li, and X. Bao, *Light: Sci. Appl.* **7**, 32 (2018).
- [27] R. Prevedel, A. Diz-Muñoz, G. Ruocco, and G. Antonacci, *Nat. Methods* **16**, 969 (2019).
- [28] S. La Cavera, F. Pérez-Cota, R. J. Smith, and M. Clark, *Light: Sci. Appl.* **10**, 91 (2021).
- [29] I. Remer, R. Shaashoua, N. Shemesh, A. Ben-Zvi, and A. Bilencia, *Nat. Methods* **17**, 913 (2020).
- [30] Y. Stern, K. Zhong, T. Schneider, R. Zhang, Y. Ben-Ezra, M. Tur, and A. Zadok, *Photon. Res.* **2**, B18 (2014).
- [31] A. Choudhary, I. Aryanfar, S. Shahnia, B. Morrison, K. Vu, S. Madden, B. Luther-Davies, D. Marpaung, and B. J. Eggleton, *Opt. Lett.* **41**, 436 (2016).
- [32] D. Zhou, P. Li, D. Ba, W. Hasi, and Y. Dong, *Opt. Lett.* **47**, 3211 (2022).
- [33] K. Y. Song, W. Zou, Z. He, and K. Hotate, *Opt. Lett.* **33**, 926 (2008).
- [34] Z. Zhu, D. J. Gauthier, and R. W. Boyd, *Science* **318**, 1748 (2007).
- [35] A. Kobayakov, M. Sauer, and D. Chowdhury, *Adv. Opt. Photon.* **2**, 1 (2010).
- [36] X. Tu, Q. Sun, W. Chen, M. Chen, and Z. Meng, *IEEE Photonics J.* **6**, 6800908 (2014).
- [37] R. Chu, M. Kanefsky, and J. Falk, *J. Appl. Phys.* **71**, 4653 (1992).
- [38] H. Wang, D. Ba, X. Mu, D. Zhou, and Y. Dong, *IEEE J. Sel. Top. Quantum Electron.* **27**, 1 (2021).
- [39] E. Hewitt and R. E. Hewitt, *Arch. Hist. Exact Sci.* **21**, 129 (1979).
- [40] R. Bonifacio, R. M. Caloi, and C. Maroli, *Opt. Commun.* **101**, 185 (1993).